AGU ADVANCING EARTH AND SPACE SCIENCES

Geophysical Research Letters

RESEARCH LETTER
10.1029/2025GL114746

The Near-Surface Boundary Layer of Hurricane Laura (2020) at Landfall

Karen Ann Kosiba[1], **Joshua Wurman**[1], **and Paul Robinson**[1]

[1]University of Alabama in Huntsville, Huntsville, AL, USA

Key Points:

- Winds and turbulent kinetic energy are maximized in the hurricane eyewall, where boundary layer rolls are most prominent and vigorous
- Three-dimensional boundary layer rolls three-dimensional structures act to bring down stronger winds from aloft toward the surface

Supporting Information:

Supporting Information may be found in the online version of this article.

Correspondence to:

K. A. Kosiba,
kakosiba@uah.edu

Citation:

Kosiba, K. A., Wurman, J., & Robinson, P. (2025). The near-surface boundary layer of Hurricane Laura (2020) at landfall. *Geophysical Research Letters*, *52*, e2025GL114746. https://doi.org/10.1029/2025GL114746

Received 16 JAN 2025
Accepted 21 APR 2025

Abstract While challenging, quantification of the near-surface landfalling hurricane wind field is necessary for understanding hurricane intensity changes and damage potential. Using single- and dual-Doppler Doppler on Wheels and in situ anemometer data, the wind structure of the very near-surface boundary layer of Hurricane Laura (2020) is characterized. Small-scale hurricane boundary layer (HBL) rolls (HBLRs) with a median size of approximately 400 m are present throughout much of the landfall, but are most vigorous in the eyewall. The maximum turbulent kinetic energy (TKE) and momentum flux associated with HBLRs occur in the eyewall and are much larger than previously documented at landfall. DOW-derived and anemometer-derived TKE values are comparable. Observed maximum surface gusts were consistent with the maximum radar wind speeds aloft, suggesting the importance of vertical transport within the HBL by sub-kilometer scale structures for the enhancement of surface wind speeds.

Plain Language Summary Landfalling hurricanes pose a significant danger to life and property. Previous studies primarily have focused on hurricane structure over the open ocean and/or in weakening landfalling hurricanes. Analysis of high-resolution mobile radar data and anemometer data near the point of landfall of Category-4 Hurricane Laura provided a unique opportunity to examine the evolution of the overland near surface winds in a major hurricane. The strongest winds aloft and near the surface occur in the hurricane eyewall, when small-scale three-dimensional structures were most prominent and vigorous. Results suggest that these three-dimensional structures act to bring down stronger winds from aloft toward the surface.

1. Introduction

Characterizing the near-surface winds in hurricanes is critical to understanding hurricane intensity changes and damage potential. Coherent structures in the near-surface hurricane boundary layer (HBL) generally are either linear, such as streaks and rolls (e.g., Kosiba, Wurman, Masters, & Robinson, 2013 (K13); Lorsolo et al., 2008 (L08); Morrison et al., 2005 (M05); K. A. Kosiba and Wurman 2014 (KW14)), Wurman & Winslow, 1998 (WW98) or vortical, such as mesovortices (e.g., Alford et al., 2019 (A19); Corbosiero et al., 2006; Hendricks et al., 2012; Kossin & Schubert, 2004; K. A. Kosiba and Wurman 2009; Reasor et al., 2009; Wingo & Knupp, 2016; Wurman & Kosiba, 2018 (WK18)), kilometer-scale vorticity enhancements inside the radius of maximum winds (Aberson et al., 2006; Marks et al., 2008), and well-resolved tornado-scale vortices in the eyewall (TSV) (WK18).

Linear HBL structures have been the focus of several observational (e.g., Guimond et al., 2018; K13; KW14; L08; M05; WW98; Zhang et al., 2008) and theoretical and numerical modeling studies (e.g., Foster, 2005; Gao et al., 2017; Gao & Ginis, 2016; Nakanishi & Niino, 2012; Zhu, 2008). These have been attributed to manifestations of "roll" circulations (Foster, 2005; L08; M05; WW98), termed HBL rolls (HBLRs), but, to date, through fine-scale dual-Doppler analyses, only KW14 has shown the three-dimensionality of these structures near the surface. Fine-scale, single-Doppler mobile radar analyses revealed characteristic wavelengths from about 300 to 500 m, depths of at least 500 m, and associated perturbation wind speeds commonly ranging from about 6 to 10 m s^{-1} (K13; KW14; L08; WW98). Studies based on WSR-88D (M05), land-based anemometry (Zhu et al., 2010), in situ aircraft (Zhang et al., 2008, 2010), and airborne radar (Guimond et al., 2018) identified slightly larger linear/roll features, with dominant wavelengths from about one to a few kilometers. Sampling resolution and altitude impact these values, but there is a coexistence of coherent scales in the HBL, with some smaller scale features closer to the surface (e.g., L08; KW14).

A consequence of the coherent structures is the distribution of momentum and turbulent kinetic energy (TKE) within the HBL. Characteristic values of vertical momentum and TKE in the HBL have been examined using

airborne data over the open ocean, and found the largest turbulence activity to occur in the eyewall. Using flight level in-situ data at 450 m altitude, Zhang et al. (2010) found TKE and eddy momentum fluxes an order of magnitude larger in the eyewall than outside. Analysis of airborne radar data from multiple hurricanes (Lorsolo et al., 2010; Rogers et al., 2012), depicted the largest TKE values in the eyewall (15–20 $m^2 s^{-2}$) and secondarily in the HBL. Guimond et al. (2018) also found the largest eddy momentum flux to occur in the eyewall (the exact location depended upon the stage of the eyewall replacement cycle). In the extreme case, vertical momentum fluxes approached 150 $m^2 s^{-2}$, but these corresponded to upward motion, contrary to assertions (e.g., WW98) that higher momentum air is mixed downward, toward the surface. Data used in airborne studies either did not extend to within, or did not adequately resolve, the flow within a few hundred meters of the surface. Observations focusing on turbulence quantities specifically due to HBL coherent structures at landfall are sparse. Using single-Doppler WSR-88D data, M05 calculated momentum flux due to HBLRs resolved in their analysis and found the average HBLR momentum flux was 8 $m^2 s^{-2}$, but maximum values approached 50 $m^2 s^{-2}$. Using dual-Doppler analyses derived from fine-scale mobile radar observations, KW14 analyzed HBL turbulent fluxes in sub-kilometer scale HBLRs and reported values comparable to the results of M05, but with variations in height and location within the hurricane.

Understanding how these HBLRs and turbulent processes manifest at the surface is necessary for accurately assessing near-surface wind hazards at landfall. Studies suggest that the maximum HBL winds aloft (defined differently in various studies) are similar in magnitude to the maximum 3-s, 10-m above ground level (AGL) gusts, with the 3-s, 10-m AGL gusts rarely exceeding this maximum HBL value (e.g., Giammanco et al., 2012, 2013, 2016; Krupar et al., 2016; Powell et al., 2003; WW98). In order for these stronger winds aloft to reach to the surface, mixing and/or transport in the HBL is necessary. Over open water, the strongest winds may occur ~500 m AGL (e.g., Alford et al., 2020; Hirth et al., 2012; Zhang et al., 2011), but the height of these maximum winds is complicated by the development of internal boundary layers at abrupt roughness changes (i.e., the coastal interface) and location within the hurricane (Giammanco et al., 2013; Kepert, 2006).

This manuscript examines the evolving near-surface boundary layer winds using fine-scale resolution mobile radar and in situ anemometer data as Category-4 Hurricane Laura made landfall. This is the first time the four-dimensional fine-scale near-surface wind field has been characterized for a landfalling Category-4 hurricane. With the exception of KW14, previous mobile-radar-based dual-Doppler analyses primarily focused on larger-scale HBL features and/or processes, not smaller-scale, nearer-to-the-surface coherent structures. KW14 examined the three-dimensional evolution of coherent HBL features in a weakening Category-2 landfalling hurricane, but the representativeness of these findings across hurricanes of various intensities, evolution, and wind regimes is unknown.

Landfalling intense hurricanes are uncommon, but likely cause the most substantially negative impacts to both coastal and inland communities due to the damaging winds and storm surge. Fine-scale sampling at landfall during such storms is challenging due to both their infrequency and the near-coastal hazards they pose. The fine-scale sampling of Hurricane Laura provides an especially valuable opportunity to characterize the properties of the HBL in an intense landfalling hurricane, increasing our understanding of how these intense hurricanes cause damage, and what modulates their intensification.

2. Data and Methodology

Hurricane Laura made landfall near Cameron, LA at ~0600 UTC (1AM CDT) on 27 August 2020 rated as a Category 4 by the National Hurricane Center (NHC). Just prior to landfall, it underwent a period of rapid intensification, defined by a 15 $m s^{-1}$ (30 kt) increase in intensity over a 24-hr period, which ended at about 0000 on 27 August. After this period of rapid intensification, the NHC reported a leveling off of estimated intensity until the hurricane made landfall. The strongest official overland wind speed was measured at the Lake Charles Regional Airport, where the 10-m AGL Automated Surface Observing System recorded a peak gust of 133 mph (59.5 $m s^{-1}$) at 0642 UTC and a maximum sustained wind of 98 mph (43.8 $m s^{-1}$) at 0654 UTC, before it failed. A University of Florida (UF) 10-m AGL tower (Balderrama et al., 2011) measured a peak wind gust of 132 mph (59 $m s^{-1}$) and a maximum sustained wind of 104 mph (46.5 $m s^{-1}$) at 0700 UTC, corresponding to Category 2 intensity. Closer to the point of landfall, at Holly Beach, LA, a peak gust of 153 mph (68.4 $m s^{-1}$) was reported by the public at 0533 UTC, but the height, anemometer model, and sustained wind speed measurements were not

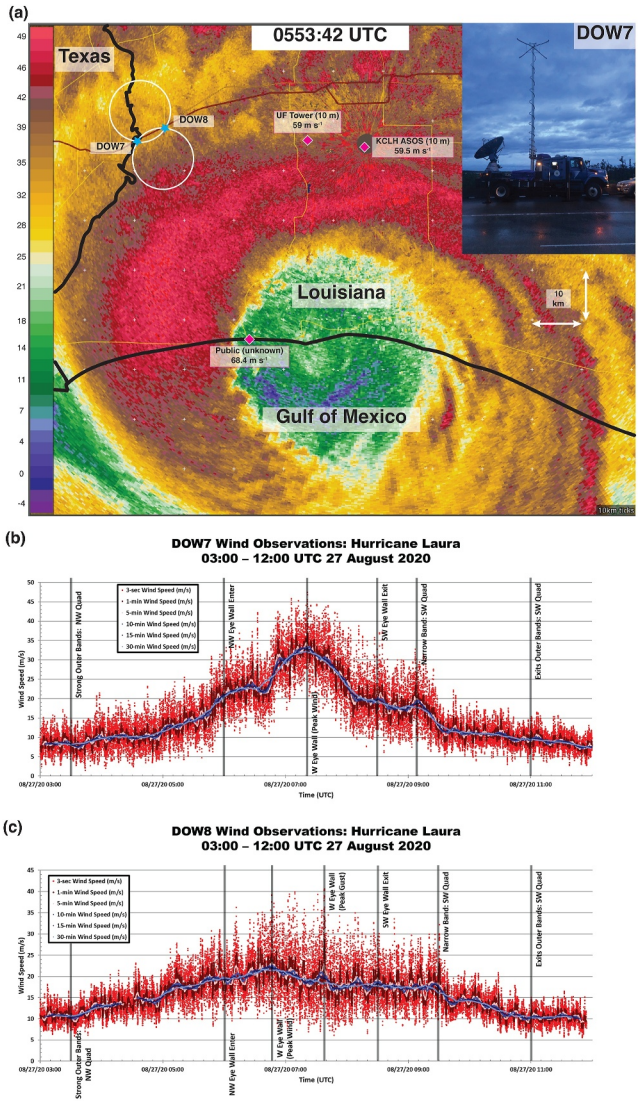

Figure 1. (a) Deployment Overview. Reflectivity from the last scan of KLCH at approximately 0554 UTC, dual-Doppler lobes between DOWs 7 and 8 (blue stars) in white, and select surface observations (magenta diamonds), and DOW7 deployment location (inset) are shown. (b) DOW7 mast anemometer wind speeds. (c) DOW8 mast anemometer wind speeds.

documented. No direct ground-based observations from well-documented instrumentation had a sustained wind speed that corresponded to a wind speed intensity above Category 2 (NHC Report 2021).

Two X-band (3-cm) Doppler on Wheels (DOW) mobile radars (Wurman et al., 2021), DOWs 7 and 8, were deployed 6.13 km apart near the point of landfall (Figure 1a). Data were collected from 0010 to 1120 UTC on 27 August 2020, spanning the entirety of the landfall period. For the majority of the deployment, both radars used a 0.333 μs (50 m) pulse with matched gating, a staggered pulse repetition frequency (Doviak & Zrnić, 1993) that resulted in a Nyquist unambiguous velocity of approximately ±60 m s^{-1} and a sampling range of ∼38 km. Data from the 0.93° physical beam width-DOWs were integrated to produce radar products such as Doppler velocity indexed at 0.5° intervals. The DOWs primarily conducted synchronized shallow volumetric scanning, from 1.0° to 5.0° or 6.0° elevation above the horizon, repeating every ∼90 s. Two consecutive 1.0° elevation scans, separated by 12 s, were conducted every 180 s.

The Velocity Azimuth Display (VAD) methodology (Browning & Wexler, 1968) was used to derive horizontal (*u, v*) winds as a function of height and time using 5° elevation radar scans. Following the methodology employed in KW14, fast-Fourier transforms (FFTs) were calculated using the 2° elevation sweeps, at 2 km range, corresponding to a height of ∼100 m above radar level (ARL), to ascertain the dominant HBL structure wavelengths for different locations within the hurricane (e.g., eyewall, rainband). Dual-Doppler (e.g., Armijo, 1969) analyses were conducted at representative times during landfall to derive the three-dimensional winds using the methodology documented in Kosiba, Wurman, Richardson, et al. (2013). To correct for the movement of wind field structures between consecutive elevations in a radar volume (features can propagate/translate ∼3,000 m during the 90-s period required to complete a radar volume), the propagation velocity (V_p) of these features was calculated. DOW radar data were objectively analyzed to a Cartesian grid using a 2-pass Barnes scheme (Barnes, 1964; Majcen et al., 2008), correcting for V_p. In order to preserve near-surface, small-scale features, a subset of the dual-Doppler domain was used. Based on the resolution at 5.7 km, anisotropic smoothing (κ) of 0.0044 km^2 (0.018 km^2) in the horizontal (vertical) and a second pass convergence parameter (γ) of 0.3 were used. The analysis domain extended 3 km horizontally and 0.5 km vertically with horizontal and vertical grid spacing of 0.025 km.

TKE and turbulent momentum flux at 100 m ARL were calculated as follows:

$$TKE = \frac{1}{2}\left(\overline{u'^2} + \overline{v'^2} + \overline{w'^2}\right)$$

$$\tau = \left(\overline{u'w'}^2 + \overline{v'w'}^2\right)^{1/2}$$

where $\overline{u'}, \overline{v'}, \overline{w'}$ are smoothed perturbation wind components in the *x*, *y*, and *z* directions, respectively. In order to compare TKE and τ values to lower resolution analyses, including models, and to exclude spurious individual data points, TKE and momentum flux were calculated at 100 m ARL over a domain-centered 2-km box, yielding 80 × 80 samples.

Each DOW was equipped with a mast-mounted RM Young 05103 anemometer, measuring horizontal wind speed and direction at 1 Hz. The height of the DOW7 mast was 20 m AGL (10 m ARL) and the DOW8 mast was 16 m AGL (8 m ARL). Using a 60-s averaging interval, TKE was calculated using just the horizontal wind components (TKE_p), assuming isotropy for the unobserved vertical component (TKE_i).

10.1029/2025GL114746

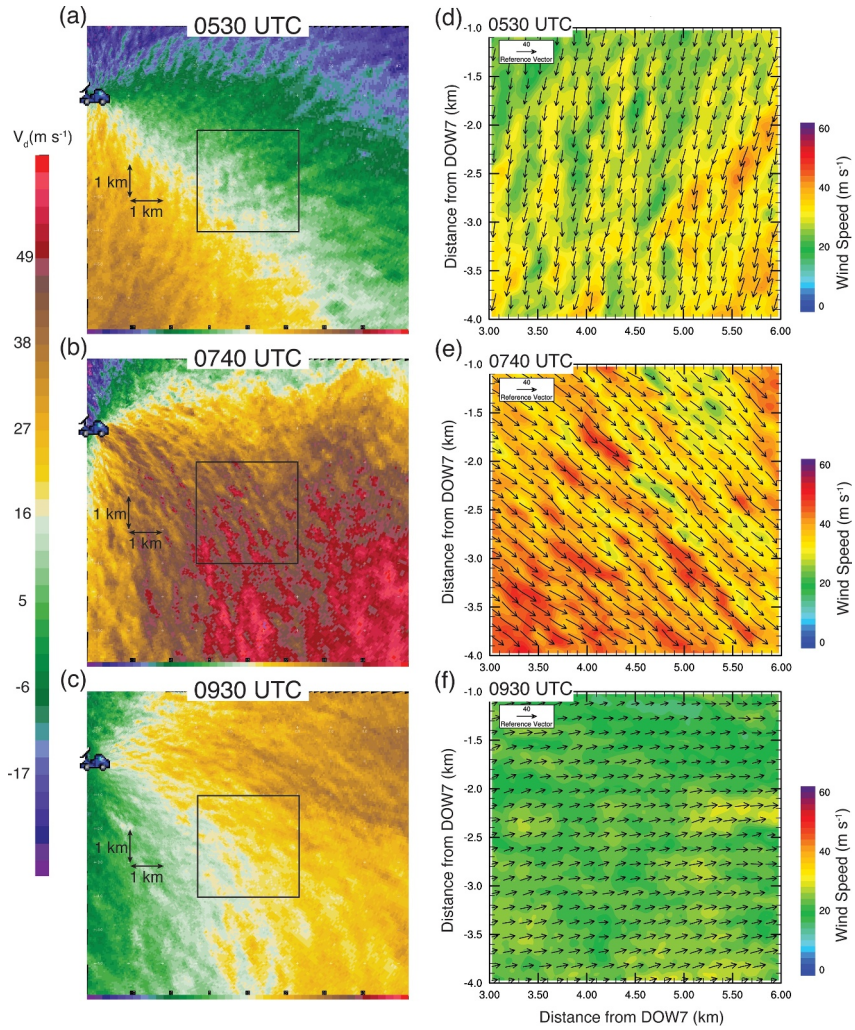

Figure 2. Doppler Velocity from DOW7 at (a) 0530 UTC, (b) 0740 UTC, and (c) 0930 UTC. The black square depicts the dual-Doppler domain. The radar icon depicts the location of DOW7. Dual-Doppler analyses at 100 m above radar level at (d) 0530 UTC, (e) 0740 UTC, and (f) 0930 UTC. Black arrows depict the horizontal winds and color contours depict the horizontal speed magnitude.

3. Results

Time series of the wind speeds and directions from the anemometers were partitioned into descriptive segments, based on locations of the observations within the hurricane (Figures 1b and 1c). The maximum 3-s wind gust at DOW7 was 48.2 m s^{-1} (108 mph) at 0721 UTC, and 43.1 m s^{-1} (96 mph) at DOW8 at 0738 UTC. At both DOW locations, the maximum wind gusts occurred in the eyewall. The DOW anemometer winds were less than the maximum winds measured by UF, likely because the DOWs were located in the western (weaker) eyewall, whereas the UF 10-m tower was located in the eastern (stronger) eyewall at landfall. The difference of 11 m s^{-1} is consistent with the position of these observations in the center-right (UF) versus center-left (DOW) eyewalls, and the propagation speed of the hurricane at 8.1 m s^{-1}.

Throughout the observation period, from 0010 to 1120 UTC, linear HBL features were present, but varied in prominence, with the earlier and later times, those outside of the eyewall, less distinct (Figures 2a–2c; Supporting Information S1). Using the three highest energy wavelengths at each time from 0222 to 0939, FFT analyses revealed a median wavelength of ~400 m for all times. Similar to L08, K13, and KW14, there was no obvious wavelength dependence of these sub-kilometer features on the horizontal wind speed, although there was a suggestion that there was more power in the smaller wavelengths at higher wind speeds. The fractional

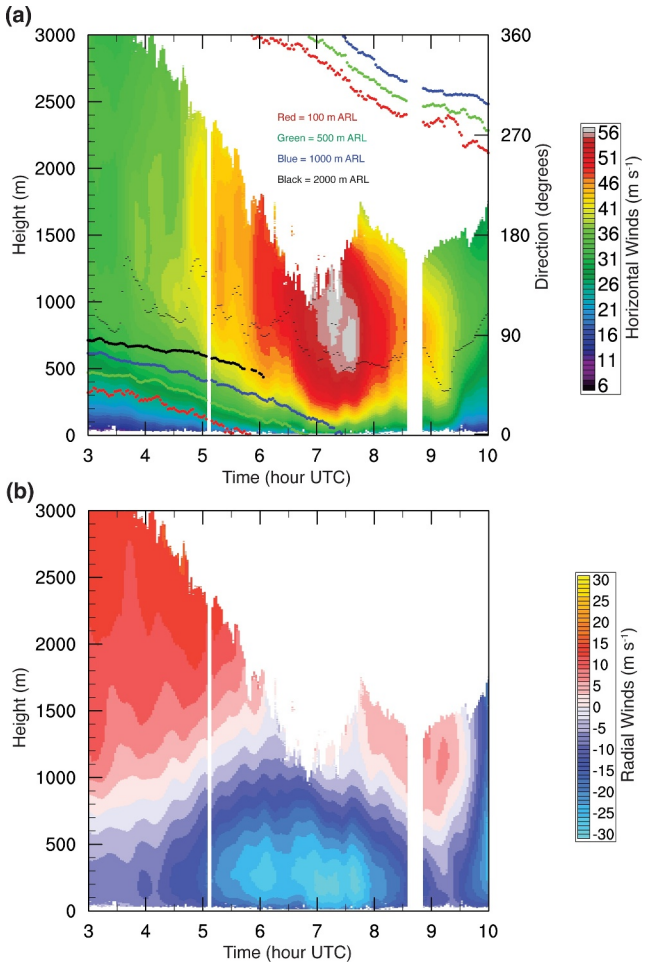

Figure 3. Velocity Azimuth Display retrievals from DOW7. (a) Color contours depict the total horizontal wind speed. Wind directions at select heights are shown with colored circles. The black dots depict the lowest height of the winds in excess of the 98th percentile horizontal wind. (b) Color contours depict the radial winds.

perturbation wind speed did not have an obvious dependence on horizontal wind speed, ranging between 10% and 15% for all times. Eyewall mesovortices (e.g., K. A. Kosiba and Wurman, 2009) were not observed, and smaller-scale vortical features, such as TSVs, previously documented in Hurricane Harvey (WK18) were not identified.

Evolution of the vertical structure of the horizontal HBL winds was examined through VAD analyses of the DOW7 Doppler winds (Figure 3). From 0300 UTC to ~0600 UTC, the maximum VAD-derived horizontal wind speed typically occurred between 0.7 and 1.8 km ARL (Figure 3a). Wind direction in the analysis domain shifted from east to north during this time. After about 0636 UTC, the height of the maximum VAD-derived horizontal winds was lower, generally between 0.7 and 1 km, with the wind direction shifting from north to west. The strongest winds occurred between about 0710 and 0740 UTC, when DOW7 was in the western eyewall. The maximum horizontal wind speed of 58 m s^{-1} occurred at a height of about 1 km ARL at 0713 UTC, close in time to when the maximum DOW and UF anemometer-measured wind speeds occurred. The maximum horizontal wind profiles were flat over a height of several hundred meters, so comparable wind speeds (within about 2–3 m s^{-1}) extended a couple hundred meters above and below the maximum wind height. To capture the lower extent of the maximum winds, the minimum height of the winds in excess of the 98th percentile horizontal wind was used (Figure 3a), and these were generally 500–700 m ARL during the eyewall.

Although the maximum VAD-derived horizontal wind speed was very similar to the maximum wind speed (59 m s^{-1}) measured by the 10-m UF anemometer, it is larger than the 48 m s^{-1} measured by the DOW7 anemometer. This difference at DOW7 between the winds aloft and the mast-measured winds likely is due, in part, to the efficiency of mixing/transporting down momentum in the HBL, which is less than 100%, and reduction in very near-surface wind speeds due to surface roughness. HBL depth, estimated from the height of the radial inflow layer (e.g., Zhang et al., 2011), ranged from ~600 to 1700 m ARL throughout the analysis period (Figure 3b). The radial wind maximum ("nose") occurred below 400 m for all analysis times. Peak inflow values of ~30 m s^{-1} occurred when DOW7 was in the eyewall, between 0700 and 0740 UTC. Maximum total horizontal wind speeds occurred above the inflow layer, near the top of the HBL.

Dual-Doppler analyses resolved structures similar to those observed in the single Doppler data (Figures 2d-2f). The magnitude of the dual-Doppler-derived perturbation horizontal speed varied, with largest median values at 100 m ARL of 5–6 m s^{-1} occurring in the 0630, 0700, and 0740 UTC analyses, in the western eyewall, although larger individual values were about 10 m s^{-1}. The fractional perturbation horizontal wind speed was correlated (+0.77) with the total horizontal wind speed, but the fractional perturbation wind speed only varied from 10% to 15%. Vertical cross sections through the linear features revealed updraft and downdraft structures, with sub-kilometer spacing, extending through the depth of the analysis domain (Figure 4a). This further supports assertions from single-Doppler analyses (e.g., WW98; M05; L08) and limited three-dimensional analyses (KW14) that, at least some of, these sub-kilometer linear structures regularly observed in single-Doppler data are manifestations of horizontal vortices. Due to the shallowness of the dual-Doppler domain, the coherency of these 3D structures above ~500 m is not conclusively revealed, but it appears the aspect ratio is ~1.

Although linear features were identified in the single-Doppler data throughout the landfall, their prominence varied with time. This variance may be reflective of a change in the structure and/or intensity, particularly the vertical, of these features. Assuming that when HBLRs are present, the downdraft (updraft) branch increases (decreases) the horizontal wind speed at a given level, the correlation between vertical winds and horizontal winds was calculated at 100 m ARL for each dual-Doppler analysis time (Figure 4b). For all times, there is a negative

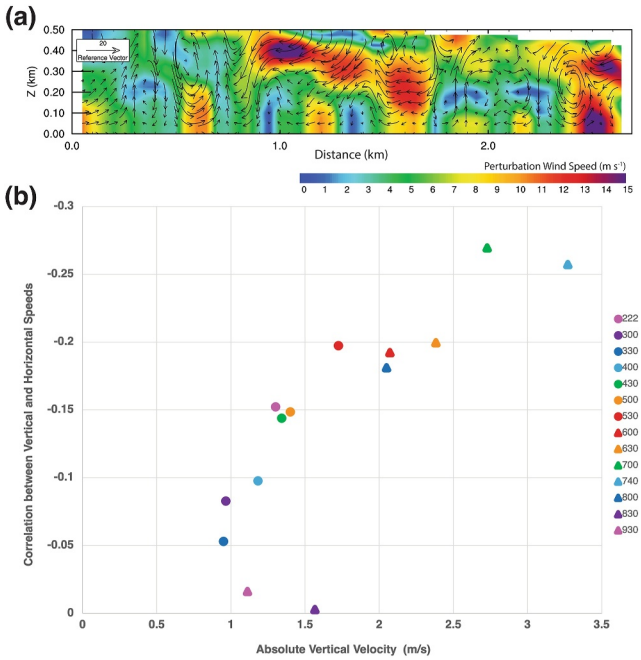

Figure 4. (a) Cross section perturbation winds at 0740. (b) Correlation between horizontal and vertical wind speeds.

correlation between the horizontal and vertical winds, implying the existence of updraft/downdraft structures, but this correlation varied with time and speed (both of which are a function of location in the hurricane). The largest absolute correlation of ∼0.26 occurred in the eyewall (0700 and 0740), while the lowest absolute correlations (<0.05) occurred after landfall, outside of the eyewall. In general, the absolute correlation increased as the eyewall approached and decreased as the eyewall departed. Using the absolute magnitude of the vertical winds as a proxy for overall strength of the updrafts/downdrafts, the larger absolute correlations were associated with stronger absolute vertical motion, implying that the HBLRs were most intense in the eyewall.

From the three-dimensional winds, TKE and vertical momentum fluxes were calculated in the different hurricane locations (e.g., eyewall) at 100 m ARL. Both TKE and vertical momentum flux varied substantially throughout the analysis domain, with individual values well over 100 $m^2\ s^{-2}$ in some locations and times, but individual localized values aren't necessarily representative. The maximum domain median TKE of ∼29 $m^2\ s^{-2}$ and the maximum domain median vertical momentum flux of 14 $m^2\ s^{-2}$ occurred at 0740, in the eyewall. Both TKE and vertical momentum flux exhibited a dependency on the median total horizontal wind speed, with correlations of 0.93 and 0.90, respectively, similar to previous findings (e.g., Zhang et al., 2010; KW14). TKE was also derived from the DOW anemometer observations (Figure 5). Depending on the assumptions (partial vs. isotropic), peak TKE values at DOW7/DOW8 approached 100/120 $m^2\ s^{-2}$. Peak anemometer-derived TKE values were similar to peak dual-Doppler-derived TKE values, and similarly occurred around the time of maximum wind, in the western eyewall.

4. Conclusions

These results depict the sub-kilometer scale HBL characteristics at landfall in a major hurricane. Similar to KW14, at least some of the linear HBL features are manifestations of horizontal roll circulations. The characteristic wavelength of ∼400 m is similar to previous high-resolution single- (WW98; L08; K13) and dual- (KW14) Doppler analyses. There is growing evidence that there is a preferred scale of near-surface HBLRs in landfalling hurricanes, independent of background wind intensity. While HBLRs are present through the data collection period, they were most prominent, and most intense, during eyewall passage. The maximum retrieved vertical momentum and TKE values occurred in the eyewall, and while larger than the values reported in KW14, median values were similar to those retrieved over the open ocean, using different methods, from airborne observations (e.g., Guimond et al., 2018; Lorsolo et al., 2010; Rogers et al., 2012).

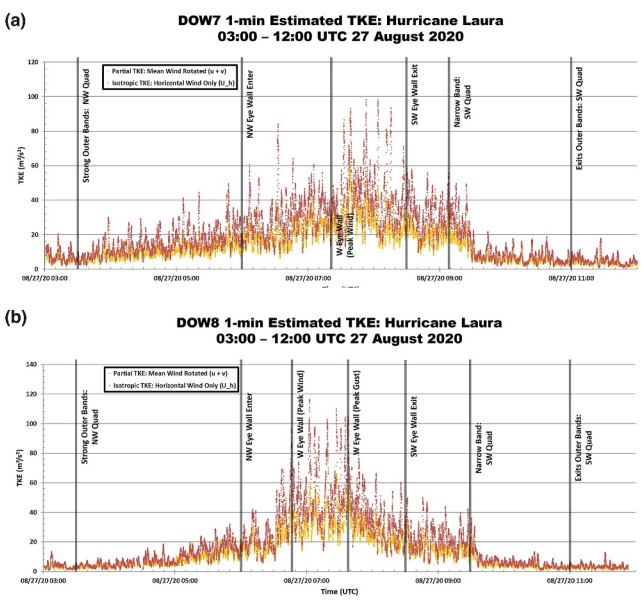

Figure 5. Turbulence kinetic energy derived from the (a) DOW7 and (b) DOW8 mast anemometers.

VAD analyses, which are representative locally and over land, showed that the height of the maximum winds in the HBL and the depth of the inflow layer decreased in the eyewall. At all times, the strongest HBL winds occurred just above the inflow layer and over a depth of several hundred meters. The overall strongest wind speeds occurred in the eyewall and wind speeds within the 98th percentile of the maximum wind speed were within 500–700 m of the surface. Even with a decrease in HBL wind speeds over land, current findings suggest that HBLRs, which are at least 500 m deep in the eyewall, bring stronger wind speeds toward the surface. The maximum gusts observed by the DOW anemometers were slightly lower than the maximum speeds aloft, but the maximum gust observed by the UF tower was very similar to the strongest winds aloft. One possibility is that the transport efficiency is not 100% and even higher winds occurred aloft near the UF tower. In addition to transport

efficiency, the complicating effects of surface roughness can substantially impact the locally observed gusts (e.g., K13), often reducing the realized surface winds. Despite Laura intensifying before landfall, other coherent boundary layer structures (e.g., TSVs) were not readily observed. While WK18 attributed the strongest gusts to TSVs in a different hurricane, the lack of TSVs in Laura suggest that maximum wind gusts may be associated with either mechanism.

Despite the growing number of observations of near-surface HBL structures, characterizing the HBL at landfall remains challenging due, in part, to the infrequency of landfalls, and sampling logistics and limitations. Case studies, especially of major hurricanes, remain important for understanding how HBL processes in a diversity of hurricane intensities impact the surface winds. Ultimately, a multi-case analysis across a broad range of intensities, surface roughness, and other factors will help put individual case studies in context, and help differentiate between the effects of wind speed regimes and locations within the hurricane on HBL structures. Many turbulent calculations depend on vertical motion, and, while dual-Doppler analyses, especially near the surface, can provide vertical wind speed estimates, future studies will benefit from using vertically pointing radars to help explicitly corroborate dual-Doppler derived vertical wind speeds.

Data Availability Statement

The radar and anemometer data used in the study are available at the permanent data repository of the Flexible Array of Radars and Mesonets (FARM) via https://doi.org/10.48514/cx9c-bv60 (Wurman & Kosiba, 2025a) and https://doi.org/10.48514/erj8-gb88 (Wurman & Kosiba, 2025b), respectively.

Acknowledgments
The analysis was supported by National Science Foundation (NSF) Grant AGS-2112980. DOWs were supported through National Science Foundation (NSF) Grant AGS-2113207. Joshua Aikins generated the mast anemometer plots in Figures 1 and 5. We thank Maiana Hanshaw for editing this manuscript, and the Hurricane Laura DOW crews that, in addition to the authors, included Andrew Frambach and Ed Grubb.

References

Aberson, S. D., Montgomery, M. T., Bell, M., & Black, M. (2006). Hurricane Isabel (2003): New insights into the physics of intense storms. Part II: Extreme localized wind. *Bulletin of the American Meteorological Society*, *87*(10), 1349–1354. https://doi.org/10.1175/BAMS-87-10-1349

Alford, A. A., Biggerstaff, M. I., Carrie, G. D., Schroeder, J. L., Hirth, B. D., & Waugh, S. M. (2019). Near-surface maximum winds during the landfall of Hurricane Harvey. *Geophysical Research Letters*, *46*(2), 973–982. https://doi.org/10.1029/2018GL080013

Alford, A. A., Zhang, J. A., Biggerstaff, M. I., Dodge, P., Marks, F. D., & Bodine, D. J. (2020). Transition of the hurricane boundary layer during the landfall of Hurricane Irene (2011). *Journal of the Atmospheric Sciences*, *77*(10), 3509–3531. https://doi.org/10.1175/JAS-D-19-0290.1

Armijo, L. (1969). A theory for the determination of wind and precipitation velocities with Doppler radars. *Journal of the Atmospheric Sciences*, *26*(3), 570–573. https://doi.org/10.1175/1520-(1969)026<0570:ATFTDO>2.0.CO;2

Balderrama, J. A., Masters, F. j., Gurley, K., Prevatt, D., Aponte-Bermúdez, L., Reinhold, T., et al. (2011). The Florida coastal monitoring program (FCMP): A review. *Journal of Wind Engineering and Industrial Aerodynamics*, *99*(9), 979–995. https://doi.org/10.1016/j.jweia.2011.07.002

Barnes, S. L. (1964). A technique for maximizing details in numerical weather map analysis. *Journal of Applied Meteorology and Climatology*, *3*(4), 396–409. https://doi.org/10.1175/1520-0450(1964)003<0396:ATFMDI>2.0.CO;2

Browning, K. A., & Wexler, R. (1968). The determination of kinematic properties of a wind field using Doppler radar. *Journal of Applied Meteorology and Climatology*, *7*(1), 105–113. https://doi.org/10.1175/1520-0450(1968)007<0105:TDOKPO>2.0.CO;2

Corbosiero, K. L., Molinari, J., Aiyyer, A. R., & Black, M. L. (2006). The structure and evolution of hurricane Elena (1985). Part II: Convective asymmetries and evidence for vortex Rossby waves. *Monthly Weather Review*, *134*(11), 3073–3091. https://doi.org/10.1175/MWR3250.1

Doviak, R. J., & Zrnić, D. S. (1993). *Doppler radar and weather observations* (2nd ed., p. 562). Academic Press.

Foster, R. C. (2005). Why rolls are prevalent in the hurricane boundary layer. *Journal of the Atmospheric Sciences*, *62*(8), 2647–2661. https://doi.org/10.1175/JAS3475.1

Gao, K., & Ginis, I. (2016). On the equilibrium-state roll vortices and their effects in the hurricane boundary layer. *Journal of the Atmospheric Sciences*, *73*(3), 1205–1222. https://doi.org/10.1175/JAS-D-15-0089.1

Gao, K., Ginis, I., Doyle, J. D., & Jin, Y. (2017). Effect of boundary layer roll vortices on the development of an axisymmetric tropical cyclone. *Journal of the Atmospheric Sciences*, *74*(9), 2737–2759. https://doi.org/10.1175/JAS-D-16-0222.1

Giammanco, I. M., Schroeder, J. L., Masters, F. J., Vickery, P. J., Krupar, R. J., III, & Balderrama, J. (2016). Influences on observed near-surface gust factors in landfalling U.S. Gulf coast hurricanes: 2004–08. *Journal of Applied Meteorology and Climatology*, *55*(12), 2587–2611. https://doi.org/10.1175/JAMC-D-16-0053.1

Giammanco, I. M., Schroeder, J. L., & Powell, M. D. (2012). Observed characteristics of tropical cyclone vertical wind profiles. *Wind and Structures*, *15*(1), 65–86. https://doi.org/10.12989/was.2012.15.1.065

Giammanco, I. M., Schroeder, J. L., & Powell, M. D. (2013). GPS dropwindsonde and WSR-88D observations of tropical cyclone vertical wind profiles and their characteristics. *Weather and Forecasting*, *28*(1), 77–99. https://doi.org/10.1175/WAF-D-11-00155.1

Guimond, S. R., Zhang, J. A., Sapp, J. W., & Frasier, S. J. (2018). Coherent turbulence in the boundary layer of Hurricane Rita (2005) during an eyewall replacement Cycle. *Journal of the Atmospheric Sciences*, *75*(9), 3071–3093. https://doi.org/10.1175/JAS-D-17-0347.1

Hendricks, E. A., McNoldy, B. D., & Schubert, W. H. (2012). Observed inner-core structural variability in Hurricane Dolly (2008). *Monthly Weather Review*, *140*(12), 4066–4077. https://doi.org/10.1175/MWR-D-12-00018.1

Hirth, B. D., Schroeder, J. L., Weiss, C. C., Smith, D. A., & Biggerstaff, M. I. (2012). Research radar analyses of the internal boundary layer over cape Canaveral, Florida, during the landfall of Hurricane Frances (2004). *Weather and Forecasting*, *27*(6), 1349–1372. https://doi.org/10.1175/WAF-D-12-00014.1

Kepert, J. D. (2006). Observed boundary layer wind structure and balance in the hurricane core. Part I: Hurricane Georges. *Journal of the Atmospheric Sciences*, *63*(9), 2169–2193. https://doi.org/10.1175/JAS3745.1

Kosiba, K., Wurman, J., Masters, F. J., & Robinson, P. (2013). Mapping of near-surface winds in Hurricane Rita using finescale radar, anemometer, and land-use data. *Monthly Weather Review*, *141*(12), 4337–4349. https://doi.org/10.1175/MWR-D-12-00350.1

Kosiba, K., Wurman, J., Richardson, Y., Markowski, P., Robinson, P., & Marquis, J. (2013b). Genesis of the Goshen County, Wyoming, tornado on 5 June 2009 during VORTEX2. *Monthly Weather Review*, *141*(4), 1157–1181. https://doi.org/10.1175/MWR-D-12-00056.1

Kosiba, K. A., & Wurman, J. (2009). High resolution and in situ observations in the hurricane boundary layer: Ike and Gustav. In *34th Conference on radar Meteorology*.

Kosiba, K. A., & Wurman, J. (2014). Finescale dual-Doppler analysis of hurricane boundary layer structures in Hurricane Frances (2004) at landfall. *Monthly Weather Review*, *142*(5), 1874–1891. https://doi.org/10.1175/MWR-D-13-00178.1

Kossin, J. P., & Schubert, W. H. (2004). Mesovortices in Hurricane Isabel. *Bulletin of the American Meteorological Society*, *85*(2), 151–153. https://doi.org/10.1175/BAMS-85-2-151

Krupar, R. J., III, Schroeder, J. L., Smith, D. A., Kang, S., & Lorsolo, S. (2016). A comparison of ASOS near-surface winds and WSR-88D-derived wind speed profiles measured in landfalling tropical cyclones. *Weather and Forecasting*, *31*(4), 1343–1361. https://doi.org/10.1175/WAF-D-15-0162.1

Lorsolo, S., Schroeder, J. L., Dodge, P., & Marks, F., Jr. (2008). An observational study of hurricane boundary layer small-scale coherent structures. *Monthly Weather Review*, *136*(8), 2871–2893. https://doi.org/10.1175/2008MWR2273.1

Lorsolo, S., Zhang, J. A., Marks, F., Jr., & Gamache, J. (2010). Estimation and mapping of hurricane turbulent energy using airborne Doppler measurements. *Monthly Weather Review*, *138*(9), 3656–3670. https://doi.org/10.1175/2010MWR3183.1

Majcen, M., Markowski, P., Richardson, Y., Dowell, D., & Wurman, J. (2008). Multipass objective analyses of Doppler radar data. *Journal of Atmospheric and Oceanic Technology*, *25*(10), 1845–1858. https://doi.org/10.1175/2008JTECHA1089.1

Marks, F. D., Black, P. G., Montgomery, M. T., & Burpee, R. W. (2008). Structure of the eye and eyewall of Hurricane Hugo (1989). *Monthly Weather Review*, *136*(4), 1237–1259. https://doi.org/10.1175/2007MWR2073.1

Morrison, I., Businger, S., Marks, F., Dodge, P., & Businger, J. A. (2005). An observational case for the prevalence of roll vortices in the hurricane boundary layer. *Journal of the Atmospheric Sciences*, *62*(8), 2662–2673. https://doi.org/10.1175/JAS3508.1

Nakanishi, M., & Niino, H. (2012). Large-eddy simulation of roll vortices in a hurricane boundary layer. *Journal of the Atmospheric Sciences*, *69*(12), 3558–3575. https://doi.org/10.1175/JAS-D-11-0237.1

Powell, M., Vickery, P., & Reinhold, T. (2003). Reduced drag coefficient for high wind speeds in tropical cyclones. *Nature*, *422*(6929), 279–283. https://doi.org/10.1038/nature01481

Reasor, P. D., Eastin, M. D., & Gamache, J. F. (2009). Rapidly intensifying Hurricane Guillermo (1997). Part I: Low-wavenumber structure and evolution. *Monthly Weather Review*, *137*(2), 603–631. https://doi.org/10.1175/2008MWR2487.1

Rogers, R., Lorsolo, S., Reasor, P., Gamache, J., & Marks, F. (2012). Multiscale analysis of tropical cyclone kinematic structure from airborne Doppler radar composites. *Monthly Weather Review*, *140*(1), 77–99. https://doi.org/10.1175/MWR-D-10-05075.1

Wingo, S. M., & Knupp, K. R. (2016). Kinematic structure of mesovortices in the eyewall of hurricane Ike (2008) derived from ground-based Dual-Doppler analysis. *Monthly Weather Review*, *144*(11), 4245–4263. https://doi.org/10.1175/MWR-D-16-0085.1

Wurman, J., & Kosiba, K. (2018). The role of small-scale vortices in enhancing surface winds and damage in Hurricane Harvey (2017). *Monthly Weather Review*, *146*(3), 713–722. https://doi.org/10.1175/MWR-D-17-0327.1

Wurman, J., & Kosiba, K. (2025a). Hurricane Laura (2020) FARM radar data. *Center for Severe Weather Research*. [Dataset]. https://doi.org/10.48514/CX9C-BV60

Wurman, J., & Kosiba, K. (2025b). Hurricane Laura (2020) FARM in situ data. *Center for Severe Weather Research*. [Dataset]. https://doi.org/10.48514/ERJ8-GB88

Wurman, J., Kosiba, K., Pereira, B., Robinson, P., Frambach, A., Gilliland, A., et al. (2021). The flexible Array of radars and Mesonets (FARM). *Bulletin of the American Meteorological Society*, *102*(8), E1499–E1525. https://doi.org/10.1175/BAMS-D-20-0285.1

Wurman, J., & Winslow, J. (1998). Intense sub-kilometer-scale boundary layer rolls observed in Hurricane Fran. *Science*, *280*(5363), 555–557. https://doi.org/10.1126/science.280.5363.555

Zhang, J. A., Katsaros, K. B., Black, P. G., Lehner, S., French, J. R., & Drennan, W. M. (2008). Effects of roll vortices on turbulent fluxes in the hurricane boundary layer. *Boundary-Layer Meteorology*, *128*(2), 173–189. https://doi.org/10.1007/s10546-008-9281-2

Zhang, J. A., Marks, F. D., Montgomery, M. T., & Lorsolo, S. (2010). An estimation of turbulent characteristics in the low-level region of intense Hurricanes Allen (1980) and Hugo (1989). *Monthly Weather Review*, *139*(5), 1447–1462. https://doi.org/10.1175/2010MWR3435.1

Zhang, J. A., Rogers, R. F., Nolan, D. S., & Marks, F. D., Jr. (2011). On the characteristic height scales of the hurricane boundary layer. *Monthly Weather Review*, *139*(8), 2523–2535. https://doi.org/10.1175/MWR-D-10-05017.1

Zhu, P. (2008). Impact of land-surface roughness on surface winds during hurricane landfall. *Quarterly Journal of the Royal Meteorological Society*, *134*(633), 1051–1057. https://doi.org/10.1002/qj.265

Zhu, P., Zhang, J. A., & Masters, F. J. (2010). Wavelet analyses of turbulence in the hurricane surface layer during landfalls. *Journal of the Atmospheric Sciences*, *67*(12), 3793–3805. https://doi.org/10.1175/2010JAS3437.1